Trait velocities reveal that mortality has driven widespread coordinated shifts in forest hydraulic trait composition

Anna T. Trugman[a,1], Leander D. L. Anderegg[b,c], John D. Shaw[d], and William R. L. Anderegg[e]

[a]Department of Geography, University of California, Santa Barbara, CA 93106; [b]Department of Ecology, Evolution and Marine Biology, University of California, Santa Barbara, CA 93106; [c]Department of Integrative Biology, University of California, Berkeley, CA 94720; [d]Rocky Mountain Research Station, US Forest Service, Ogden, UT 84401; and [e]School of Biological Sciences, University of Utah, Salt Lake City, UT 84112

Understanding the driving mechanisms behind existing patterns of vegetation hydraulic traits and community trait diversity is critical for advancing predictions of the terrestrial carbon cycle because hydraulic traits affect both ecosystem and Earth system responses to changing water availability. Here, we leverage an extensive trait database and a long-term continental forest plot network to map changes in community trait distributions and quantify "trait velocities" (the rate of change in community-weighted traits) for different regions and different forest types across the United States from 2000 to the present. We show that diversity in hydraulic traits and photosynthetic characteristics is more related to local water availability than overall species diversity. Finally, we find evidence for coordinated shifts toward communities with more drought-tolerant traits driven by tree mortality, but the magnitude of responses differs depending on forest type. The hydraulic trait distribution maps provide a publicly available platform to fundamentally advance understanding of community trait change in response to climate change and predictive abilities of mechanistic vegetation models.

community trait assemblage | drought | forest inventory | mortality | species diversity

Plant functional traits mediate tree responses to climate. Differences in local environmental conditions strongly affect which traits and community trait assemblages are successful. Community trait assemblages also directly impact ecosystem carbon uptake during average years and mortality risk and ecosystem resilience during drought events (1–4). Furthermore, community hydraulic trait composition influences land–atmosphere feedbacks by affecting water and energy fluxes from the land surface to the boundary layer (5–8). Given that it is largely unknown how ecosystems will respond to climate change and particularly climate extremes, a deeper understanding of the factors controlling trait distributions across space and time offers a mechanistic window into predicting climate change and extreme event impacts on terrestrial ecosystems and the land carbon sink.

Climate is a determinant of community trait composition as climate controls both which species occur in a community (i.e., climate constrains many species geographic ranges, see ref. 9) and the abundances of species in a given community (10). Extreme events linked to climate change have resulted in substantial shifts in species' dominance (11) and species' geographic range limits (12, 13), particularly, in water-limited biomes (13–15). Looking forward, climate extremes, such as severe droughts, are projected to increase with anthropogenic climate change (16–20) and drive increasingly dramatic shifts in plant ranges and community composition (21), and thus community trait composition. Yet, despite widespread evidence of climate-driven shifts in species' ranges (12, 22–24), we have yet to diagnose the impacts of climate change on the rates of change of many community-weighted plant traits ("trait velocities" or the trait change per

year) that influence ecosystem function, are relevant to process-based Earth system modeling, and influence plant fitness and demographic rates.

When considering the underlying mechanisms driving species' range limits, community composition, and Earth system responses to climate change, tree hydraulic traits are important because they regulate ecosystem water and carbon fluxes (25). The biophysics of stem water conductance (hydraulic conductivity through the xylem) and its drought-induced failure due to embolism are central controls on water movement through the soil–plant–atmosphere continuum (26–28). Indeed, several tree hydraulic traits have been shown to be predictive of cross-species drought mortality risk (2), and plant hydraulic transport and hydraulic traits have recently been incorporated into the vegetation model components of several Earth system models (26, 27, 29). Thus, a better understanding of the climatic and demographic processes underlying regional-scale hydraulic trait distributions and trait velocities is important to advancing predictions of future ecosystem function.

Here, we leverage the Xylem Functional Trait Database (XFT) (30) and the extensive US Forest Service Forest Inventory and Analysis (FIA) long-term permanent plot network (31), which contains >160,000 forested permanent plots across the contiguous United States, to develop high-resolution trait maps

---

Significance

Tree hydraulic traits determine plant water use and tree vulnerability to drought stress thereby affecting forest productivity and the movement of water between the land surface and the atmosphere. Here, we leverage an extensive trait database and a long-term continental forest plot network to map changes in the hydraulic traits of tree communities across the United States. We find evidence for shifts toward communities with more drought-tolerant traits driven by tree mortality. This trait compositional change may buffer forest productivity and water fluxes in the near term from the effects of climate change.

---

based on species distribution and abundance. We then used the trait maps, FIA-measured demographic rates, and 4-km spatial resolution climate data from the TerraClimate dataset (32) to quantify and diagnose the plant hydraulic trait velocities (rates of change in community-weighted traits) for forests across the United States for nearly two decades from 2000 to present. We ask: 1) how do hydraulic and photosynthetic traits vary regionally across the continental United States? 2) what environmental factors affect diversity in traits, and how does diversity in hydraulic traits relate to overall species diversity? 3) have community hydraulic trait compositions changed over the past two decades? 4) what demographic and climatic drivers are associated with these trait velocities? and 5) do responses vary by forest type or region?

Results and Discussion

We quantified spatial patterns in three hydraulic traits and one photosynthetic trait that collectively represent metrics of species' hydraulic efficiency and safety (2, 28, 33). Specifically, we considered water potential at which 50% of stem xylem conductivity is lost (P50), hydraulic safety margin (HSM), or the difference between the P50 and the minimum stem water potential typically experienced, xylem conductivity per area of leaves distal to the measured xylem segment (K_L), and maximum photosynthetic rate (A_{max}) (Fig. 1). We calculated community-weighted mean trait values based on high-resolution species distribution and abundance data from the FIA (approximately one plot for every 2,428 ha of land). We found that photosynthetic and hydraulic traits varied substantially depending on regional climatic and edaphic factors. Trait spatial patterns revealed drought-tolerant traits throughout water-limited regions: strongly negative community-weighted P50 values in juniper (*Juniperus* species) monocultures in central Texas and piñon (*Pinus edulis*)–juniper woodlands in the Mountain West region of the United States co-occurring with large HSMs (red and dark orange in Fig. 1*A* and dark blue Fig. 1*B*). A notable exception to this high HSM pattern in water-limited systems is that of velvet mesquite (*Prosopis velutina*)-dominated woodlands (the negative HSM in southern Arizona and New Mexico; light yellow, Fig. 1*B*) (34, 35). The slightly negative HSM (meaning minimum stem water potential is more negative than P50) combined with relatively high K_L (blue, Fig. 1*C*) of velvet mesquite contrasts with the strongly negative P50 and high HSM of the piñon–juniper woodlands and suggests that

the driest wooded ecosystems may employ diverse physiological strategies to cope with climate extremes. In the case of velvet mesquite and the piñon–juniper woodlands, the contrasting pattern of HSM is potentially indicative of mesquite species' well-documented deep roots, which can extend up to 50 m and provide access to perennial soil–water sources (36). Given a relatively stable deep water reservoir, a large HSM would be unnecessary for mesquite in most instances, despite sparse precipitation. The small HSMs of mesquite systems, therefore, likely indicate a decoupling of vegetation from the above-ground climate rather than high vulnerability to water stress. Finally, the sharp divide between eastern hardwoods and drought-tolerant woodlands of Texas is clearly visible in multiple physiological trait patterns (Fig. 1 *A* and *D*).

We calculated the range in traits of co-occurring species at a given FIA plot and found that the hydraulic trait breadth does not scale with overall species diversity (Fig. 2 and *SI Appendix*, Fig. S1). In particular, the much lower diversity forests in the Mountain West region of the United States, which are composed typically of two to three species, exhibited an equivalently large range of P50 and HSM values as more diverse southeastern forests (Fig. 2 *A* and *B* and *SI Appendix*, Fig. S1). This mirrors patterns of mismatching taxonomic and functional diversity in other systems (e.g., birds, ref. 37). The difference in measures of trait diversity per unit of species diversity between Mountain West and southeastern forests is likely reflective of landscape heterogeneity driven by both the heightened seasonality in rainfall and temperature in Mountain West forests and greater topographic relief (38). Climate seasonality causes temporal heterogeneity in water availability and temperature. Topographic relief can heighten climate seasonality effects and creates spatial heterogeneity in water availability, temperature, and radiation load. We hypothesize that both spatial and temporal heterogeneities facilitate the co-occurrence of different physiological strategies (37). However, since FIA plots are typically too small to capture topographic variation (and Fig. 2 shows only within-plot α diversity), temporal heterogeneity (climate seasonality) may be particularly important.

We further analyzed our trait maps to quantify changes in community-weighted P50 and HSM, two traits shown to be predictive of cross-species drought mortality patterns (26, 27). We calculated differences between the community-weighted P50 and HSM from the initial to the final FIA censuses divided by the length of the census period to quantify the trait velocity (trait
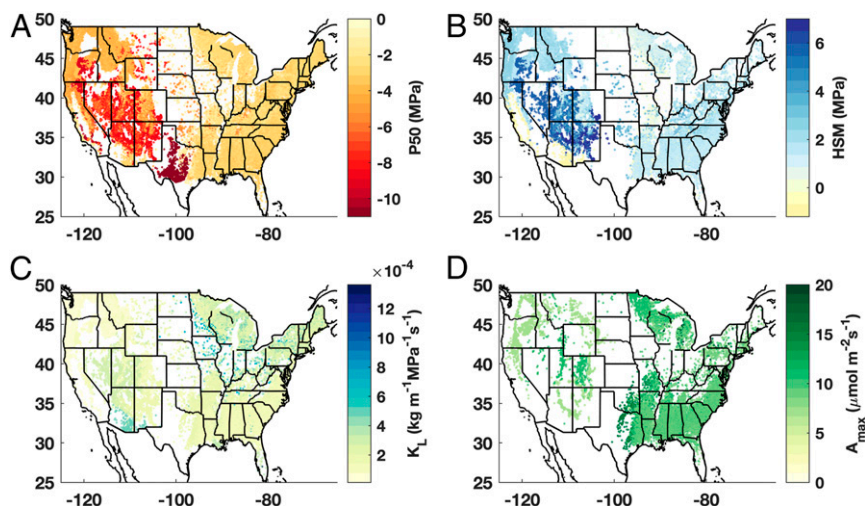
Fig. 1. Hydraulic and photosynthetic traits vary substantially across the continental United States. Spatial variations in community-weighted (*A*) water potential at which 50% of stem xylem conductivity is lost (P50), (*B*) HSM, or the difference between the minimum stem water potential typically experienced and the P50, (*C*) xylem conductivity per total area of leaves distal to the measured xylem segment (K_L), and (*D*) maximum photosynthetic rate (A_{max}). White space indicates nonforested regions or regions where trait coverage was less that 80% by stand basal area.

ECOLOGY
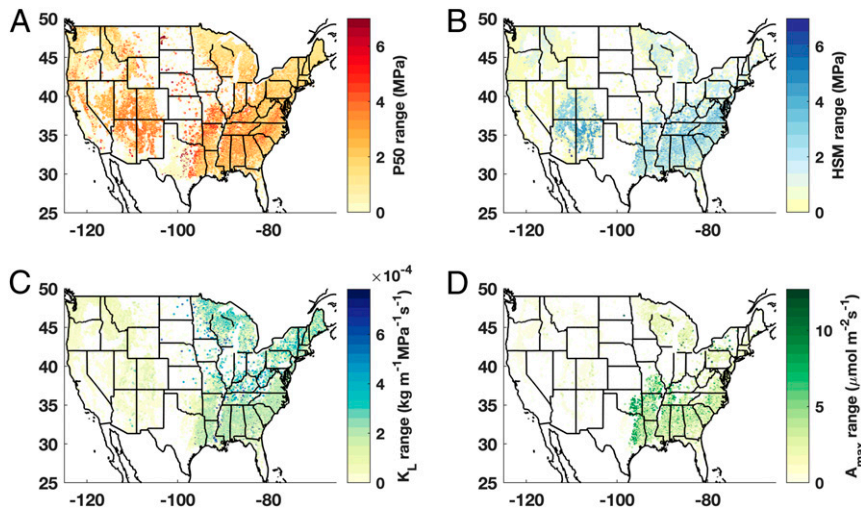
Fig. 2. Substantial diversity in hydraulic and photosynthetic traits exists and is not solely related to overall species diversity. Spatial variations in community trait range for (*A*) water potential at which 50% of stem xylem conductivity is lost (P50), (*B*) HSM, or the difference between the minimum stem water potential typically experienced and the P50, (*C*) xylem conductivity per total area of leaves distal to the measured xylem segment (K_L), and (*D*) maximum photosynthetic rate (A_{max}). White space indicates nonforested regions or regions where trait coverage was less that 80% by stand basal area. Range values of zero indicate monospecific forest plots.

change per year) in a given community and diagnosed the underlying drivers of trait change. We first examined if there were significant shifts in P50 and HSM and if changes depended on forest type (angiosperm- versus gymnosperm-dominated). We found strong evidence for a significant decrease in the inventory mean P50, driven predominantly by decreases in P50 in gymnosperm forests (*SI Appendix,* Table S1). Additionally, we found some evidence for a significant increase in the inventory mean HSM in all forests for one data filtering method and for angiosperm forests with multiple data filtering methods (*SI Appendix,* Table S1). Trait velocities of P50 and HSM are consistent with selection for more drought-tolerant communities.

We next quantified and diagnosed the P50 and HSM trait velocities over the past two decades by relating the rate of change in P50 and HSM (in MPa y^{-1}) to mortality rates (basal area in m^2 ha^{-1} y^{-1}) and year of final census in the FIA. We found significant decreases in P50 and increases in HSM in most regions and forest types were associated with local mortality rates (Fig. 3 *A–C*). Interestingly, we found evidence for significant decreases in P50 and increases in HSM in gymnosperm-dominated and western forests with measurement year, with larger changes in stands censused more recently, which could be indicative of an acceleration in the rate of change in P50 and HSM (39, 40) (*SI Appendix,* Table S2 and *Methods*).

We further examined the regional climatic drivers associated with changes in community-weighted P50 and HSM using the Terra-Climate dataset (32, 41, 42). Of the environmental drivers tested (see *Methods*), we found that CWD was most predictive of both changes in P50 and HSM over the past two decades (Fig. 3 *D* and *E* and *SI Appendix,* Table S3). Specifically, regions with a higher growing season CWD (higher aridity) experienced significant shifts over the past two decades toward community-weighted P50s that are more negative and significant shifts toward community-weighted HSMs that are larger (e.g., more drought-tolerant communities). Although broad trends existed across forest types and geographic regions, some interesting differences were apparent. For example, gymnosperm-dominated forests and forests in the western United States exhibited significant shifts toward more negative P50 and larger HSMs with increased CWD, whereas this trend was not apparent in less water-limited eastern forests (Fig. 3 *D* and *E*).

Significant decreases in P50 and increases in HSM associated with mortality were robust, even when species known to be suffering nonclimate related mortality due to pests/pathogens, or declines related to fire suppression were excluded from the analysis. We performed sensitivity tests where we examined the trait velocity-mortality relationship while excluding, in turn, *P. edulis* (piñon pine) and *Pinus contorta* (lodgepole pine), which suffered from bark beetle mortality, *Quercus alba* and *Quercus rubra* (white and red oak), which have been reported to suffer mortality resulting from due to long-term fire suppression (43), *Tsuga canadensis* (eastern hemlock), which has suffered mortality due to wooly adelgid, and *Fraxinus pennsylvanica* and *Fraxinus americana* (green and white ash), which have been attacked by the emerald ash borer, and found no significant change between the rate of change in P50 and HSM relative to mortality rates (*SI Appendix,* Table S2). Although our analysis does not preclude other drivers from influencing forest demographic rates and traits, it indicates that climate and water availability are important drivers. Given that traits have changed more in dry places (with higher CWD), and that trait changes are associated with nonspecific mortality, our results indicate that climate-driven mortality (either proximately or through interactions with pest outbreaks, see refs. 44–46) is likely behind these trait shifts. Indeed, a similar relationship between community drought tolerance and water limitation has been observed even in the wetter eastern forests of the United States after accounting for confounding factors, such as forest age and anthropogenic harvesting (47). We cannot rule out nonclimatic factors, such as rising CO_2, invasive pests, and legacies of fire suppression. However, if nonclimate factors are the main drivers of P50 and HSM trait velocities, they, at least, appear to be making US forests more drought tolerant.

Finally, we found that changes in HSM and P50 were coordinated, regardless of forest type such that forests with a decrease in community-weighted P50 also often saw an increase in HSM (Fig. 4 and *SI Appendix,* Table S4). Given that HSM is defined as the difference between the P50 and the minimum stem water potential typically experienced, coordinated shifts in community mean HSM and P50 are indicative that minimum stem water potential tends to decrease proportionally with P50. Globally, P50 and HSM are only partially correlated across
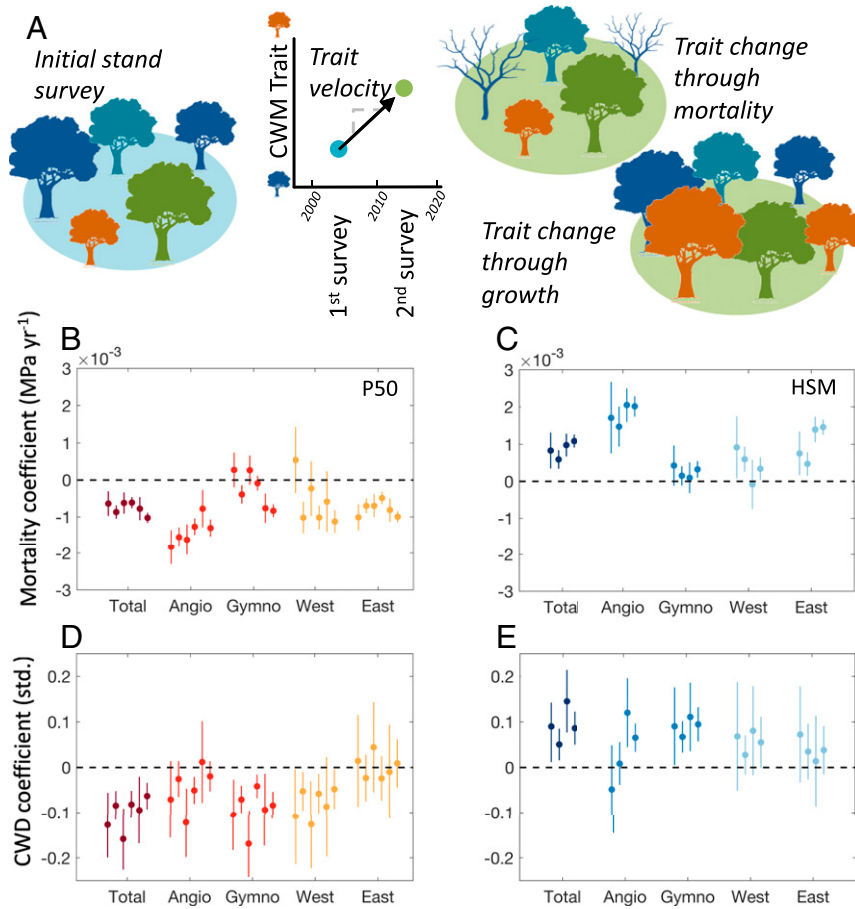
Fig. 3. Shifts in community trait composition toward more drought-resistant forests are associated with mortality and aridity but differ substantially depending on region and forest type. (*Top*) Schematic of the mechanisms resulting in shifts in community weighted mean (CWM) trait composition and the subsequent trait velocities including trait change through selective recruitment and growth or through selective mortality of trees with particular traits (*A*). Different colors represent different species with distinct trait values. (*Middle*) Response coefficient between forest basal area mortality and community-weighted changes (final minus initial inventory divided by inventory interval length) in key drought tolerance traits including (*B*) water potential at which 50% of stem xylem conductivity is lost (P50) and (*C*) HSM for the inventory as a whole (Total), angiosperm forest types (Angio), gymnosperm forest types (Gymno), the eastern United States (East), and the western United States (West). (*Bottom*) Standardized response coefficients between climatic water deficit (CWD) and community-weighted changes (final inventory minus initial inventory) in (*D*) P50 and (*E*) HSM. CWD is calculated for mean growing season (May–August) for the inventory interval. For *B–E*, grouped points are response coefficient estimates using different data gap filling and outlier screening methods (see *Methods*). Similar forest types are grouped by color, error bars show 95% confidence intervals, and associated significance levels are in *SI Appendix*, Tables S2 and S3.

species (ρ = −0.54 across 577 species in the XFT database with measures of both traits), meaning that increased drought tolerance (P50) and increased relative safety (HSM) do not necessarily go hand in hand. However, among dominant North American forest tree species, there is a strong correlation between P50 and HSM (ρ = −0.78 across 55 species with measures of both traits), which, no doubt, drives the coordinated shifts in community mean P50 and HSM found here. Persistent changes toward more negative community-weighted P50s and larger community-weighted HSMs have important implications for the resilience of US forest communities in coming decades. P50 is indicative of the amount of hydraulic stress a tree can sustain before suffering hydraulic damage, so communities with more negative P50s are expected be more resilient to increased routine water stress. Communities with larger HSMs may additionally be more able to withstand increased variability in water stress because of a larger buffer between the expected seasonal water stress and the amount of stress that induces costly and potentially lethal hydraulic damage. Coordination between HSM and P50 trait velocities indicates that forests may be more able to withstand both a more stressful mean climate and increased climate variability and/or extremes.

While our results quantify trait velocities associated with shifts in species composition documented in forest inventory plots, we note that substantial intraspecific variation in plant traits exists (48–50) and could be important to include in future regional trait distribution estimates. We hypothesize that the mechanisms driving intraspecific variation in traits, such as trait plasticity and/or genetic variation have the potential to further buffer ecosystems to novel climate conditions on top of changes in species composition. Furthermore, HSM can be a challenging trait to quantify because the minimum water potential measurement (used in the calculation of HSM) is influenced by individual study context and design, such as whether annual or interannual minimum water potentials were reported and the severity of water limitation during the period over which measurements were collected. In our analysis, we were limited to the definition used by the database compilers who define HSM as "the difference between the P50 and the minimum stem water potential observed for a species" (51) rather than the difference between the P50 and the minimum stem water potential during a period of extreme water limitation as would occur during a drought. Thus, interpretation of HSM results, particularly, between the eastern and the western US forests, should be performed with
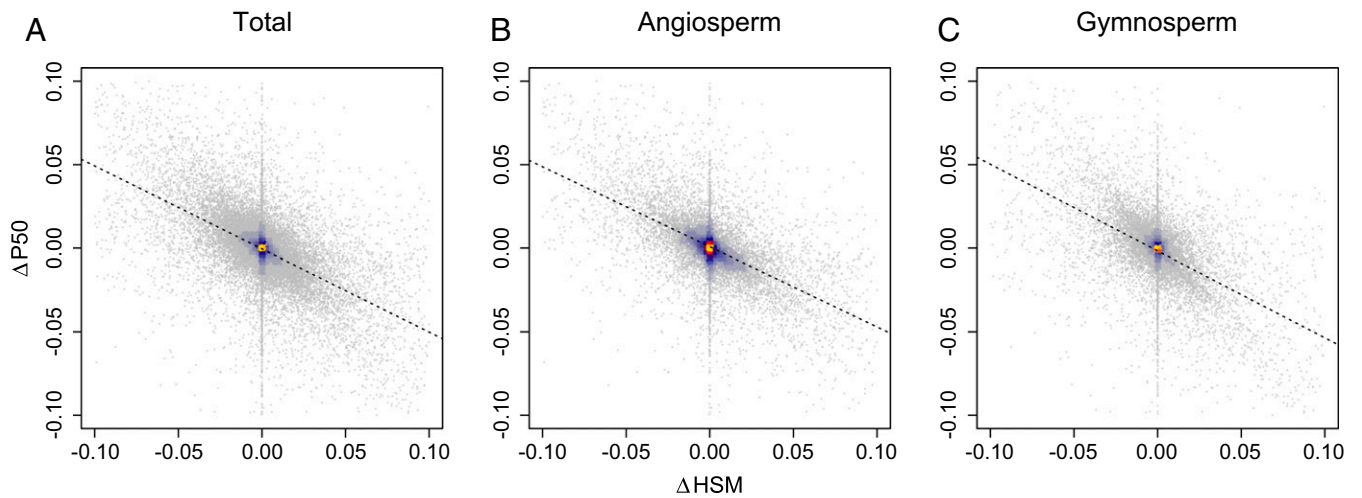
Fig. 4. Trait velocities between HSM and water potential at which 50% of stem xylem conductivity is lost (P50) are coordinated. Shifts in P50 and HSM (MPa y^{-1}) for (*A*) the inventory as a whole, (*B*) angiosperm forest types, and (*C*) gymnosperm forest types. Each point represents an individual plot with at least 80% trait coverage by basal area in the initial inventory, and hotter colors indicate a higher density of points. Dashed black lines show the ordinary least-squares regression line of best fit. Spearman's ρ and associated significance levels are in *SI Appendix*, Table S4.

caution because long-term trends indicate a stronger intensification in water limitation in the western United States compared to the eastern United States over the past several decades (52), potentially resulting in a systematic bias in HSM estimates.

With this analysis, we developed open source trait maps that can serve as a platform for mechanistic vegetation models to improve geographic trait distributions for the continental United States (53). Furthermore, we provide quantitative evidence for coordinated changes in community-weighted mean P50 and HSM across the United States over the past two decades, indicating that forest communities have experienced compositional shifts toward more drought-tolerant ecosystems since 2000. We found that these shifts were larger in drier regions and were associated with tree mortality. The concept of trait introduced in this analysis has utility beyond quantifying the degree to which functional change has occurred in a given community. Trait velocities have the potential to mechanistically link communities' "trait space" with the prediction of forest mortality risk by identifying mismatches in the rate of community trait adaptation and the rate of climate change (54). Through the use of trait velocities and plant hydraulic trait maps in hydraulically enabled trait-based vegetation models, it should now be possible to rigorously partition the relative importance of ecology (i.e., shifts in species composition and the impact on community hydraulic traits) versus environment (changes in mean climate and climate variability) on the terrestrial carbon cycle. Such partitioning could inform both future conservation efforts as well as climate change adaptation and mitigation strategies.

Methods

Forest Inventory and Analysis Data. We used the US Forest Service FIA long-term permanent plot network to generate high-resolution hydraulic and photosynthetic trait maps for the continental United States based on species composition and abundance and to document and diagnose the evolution of trait distributions across the United States from 2000 (when FIA protocols were standardized nationwide) to the present. The FIA plots are set up on a stratified systematic sampling design using a hexagonal cell grid (55). The network contains >160,000 permanent plots sampling forests where tree status (living/dead) is measured on a plot return interval that varies by state, typically, every 5 to 10 y. Within plots, different condition classes can be mapped and recorded separately, representing different land cover class types, size classes, or other distinguishing characteristics. In our analysis, we excluded plot-condition groupings with fire damage, human damage, or other treatments so that we could isolate the effects of climate on the dynamics of community trait compositions. Given that condition classes with a small plot fraction can overinflate forest basal area, we examined a plot of

forest basal area as a function of condition class plot fraction and found that a forest condition class threshold >30% of an individual plot's area was the minimum threshold that filtered large basal area anomalies. Thus, we required a forest condition class to occupy >30% of a given plot's area to be included in the analysis.

Maps of Community-Weighted Trait Distributions and Trait Diversity. We calculated community-weighted mean trait values, community trait range, and quantified decadal-scale changes in community-weight traits between the final and the initial inventory census by pairing plot-level species basal area abundance derived from the FIA with plant hydraulic and photosynthetic trait data from the XFT database (30). Plant hydraulic traits included the water potential at 50% loss of hydraulic conductivity (P50), HSM, and xylem conductivity per area of leaves distal to the measured xylem segment (K_L). We mapped hydraulic traits in conjunction with maximum photosynthetic rate (A_{max}; µmol m^{-2} s^{-1}). For species with multiple trait observations within the XFT (*SI Appendix*, Fig. S2), we computed species' means and included a number of sensitivity analyses to account for method uncertainties in hydraulic trait measurements (see below). This methodology neglects intraspecific variation due to environment or tree life stage (48–50). While maps based on species mean values will not capture the full spectrum of hydraulic and photosynthetic trait variabilities, they offer considerable added information above basic species composition and provide an important platform for understanding how and why traits vary across space and time. Furthermore, it has been shown that species-level averages are predictive of plant performance during and after drought (2, 3).

In our analysis, we included several measurement screening criteria for data quality control in the XFT, data gap filling techniques, and to address ongoing uncertainties in the plant hydraulics literature related to measuring P50 (56). For the majority of analyses of P50, the calculation of HSM, and phylogenetic imputing (described below), we performed the following additional quality control on the data available in the XFT. We i) only used P50s derived from branches (no petioles, leaves, or roots) and ii) filtered for strongly R-shaped vulnerability curves (where we excluded P50 measurements >−0.75 MPa, measurements with HSM <−2 MPa, and any measurements where gravitational effects due to tree height were within 0.5 MPa of P50). We refer to this, subsequently, as our "base-version trait dataset." Additionally, we performed a separate analysis on a conservative end-member estimate of P50 measurements where we strictly selected for sigmoidal vulnerability curves to avoid any artifacts associated with long-vesseled species (57) resulted in coverage of only 91 species. We refer to this, subsequently, as the "strict quality control version." Finally, given the evidence for a considerable phylogenetic signal in many plant traits (58, 59), we developed a separate trait dataset where we phylogenetically imputed missing traits based on genus means for genera with more than two measured species to increase trait coverage. Subsequently, we refer to this version as the "phylogenetically imputed trait dataset." As a slightly more conservative imputation, we removed imputed values in genera with the top 25% highest within-genus CVs for each trait (SD was used for HSM), under

Trugman et al.

the assumption that these genera likely showed the least phylogenetic signal useful for trait imputation. Results were qualitatively identical when imputing with all genus means or only the least variable genera, so we present results only using the latter imputation method. Genus means were used as opposed to a more sophisticated phylogenetic imputation (e.g., ref. 58) because within-genus phylogenetic resolution was not readily available from published phylogenies accessible through ref. 60.

After data quality control, we calculated community-weighted trait values based on species basal area relative to the total plot basal area with trait coverage at a given location. We also recorded the range (max and min) in species-level mean trait values for each location with adequate trait coverage. Summaries of trait data coverage for each trait are included in *SI Appendix*, Table S5.

In all statistical analyses, except where noted, we independently analyzed our base-version trait dataset, the phylogenetically imputed version, and, for P50 only, the strict quality control version. In all cases, only plot locations with trait coverage of >80% by basal area in the initial census were included in the analyses so as to not bias results due to poor species coverage. Our results are robust to these different levels of quality control and inventory coverage (*SI Appendix*, Fig. S3 and Table S2).

Sensitivity of Community Traits to Climate and Demographic Drivers. Given that HSM and P50 have been shown to be key traits for predicting species mortality risk and productivity during periods of water limitation (2, 3), we further analyzed the change in community traits over the duration of the inventory period. We calculated the change in community-weighted mean P50 and HSM between the first and the last plot census to get ΔP50 and ΔHSM and looked at trait sensitivities for the inventory across the entire United States as well as by forest type (angiosperm versus gymnosperm) and geographic location (eastern versus western United States). To categorize plots as angiosperm-dominated or gymnosperm-dominated forests, we used the FIA "field type code" variable. Eastern and western plots were divided by state with the dividing line running west of Minnesota to Louisiana. Finally, we performed a series of sensitivity tests to see if factors other than climate, such as pest, pathogen, or anthropogenic fire suppression, were major drivers of tree mortality by excluding plots dominated by species known to be associated with these factors. Specifically, plots dominated by *P. edulis* (piñon pine), *P. contorta* (lodgepole pine), *Q. alba*, and *Q. rubra* (white and red oak), *T. canadensis* (eastern hemlock), and *F. pennsylvanica* and *F. americana* (green and white ash) were excluded each, in turn, based on the plot FIA field type code. Collectively, these sensitivity tests help unpack if known species suffering from severe bark beetle outbreaks (pines), potential oak mortality due to long-term fire suppression (43), mortality due to wooly adelgid (hemlock), and mortality due to the emerald ash borer are driving significant relationships between HSM/P50 and mortality.

First, we looked for significant shifts in population mean trait distributions in P50 and HSM between the first and the last inventory using the Wilcoxon signed-rank test (given the lack of normality in trait distributions). Next, to analyze trait responses to climate, we used climate variables from the TerraClim dataset (32), which includes a number of climate metrics from 1956 to 2018 at a monthly time step and 4-km spatial resolution globally. We initially tested a wide suite of climate variables including,CWD, the Palmer Drought Severity Index (PDSI), precipitation, snow water equivalent, soil moisture, daily maximum temperature averaged to the monthly level (T_{max}), and atmospheric vapor pressure deficit (VPD). For each grid cell associated with a FIA plot, we computed the growing season average (defined as June–August given that all plots are in the Northern Hemisphere) averaged over the interval between the first and the last census (which varies by plot according to the state-specific remeasurement interval), growing season extreme (minimum for PDSI and soil moisture and maximum for CWD, T_{max}, and VPD) over the census interval, and climatic anomaly (excluding PDSI which is, by definition, already an anomaly) over the census interval relative to both 20-y and 30-y climatologies spanning from 1997 or 1987 to 2017, respectively. For snow water equivalent only, we summed the entire water year (October–September) and computed the census interval average, minimum, and anomaly.

Initial climate variable selection was based on three criteria: i) a lack of collinearity, ii) biologically relevant climate stressors that capture multiple elements of drought stress, and iii) a model selection algorithm that selected climate predictors that showed significant associations with ΔP50 and ΔHSM. We grouped predictors into categories of growing season means, extreme, and anomalies (because, in many cases, means and extremes were highly correlated). For each group, following standard approaches to deal with collinear predictor variables, we first used a matrix of pairwise correlations and removed any variable with high correlations ($R > 0.5$) with other predictor variables. Each pairwise correlation was performed, and the variable with the lower correlation with the dependent variable was removed. We further verified that variance inflation factors were less than 2.5 for all predictor variables. This resulted in four climate predictor variables in each mean, extreme, and anomaly category, CWD (a metric of total water availability), PDSI (a metric of drought stress), soil moisture (a metric of root zone water availability), and VPD (a metric of atmospheric dryness). Mean CWD over the census interval proved to be most explanatory compared to other predictors, extremes, or anomalies, so we opted to look at the sensitivity of ΔP50 and ΔHSM to CWD.

We quantified the regional-scale sensitivity of cumulative changes in P50 and HSM to CWD by upscaling the data to 1.0° using grid-specific mean ΔP50/ΔHSM and grid-specific mean CWD according to the methods of ref. 47. We used linear models and confirmed that there was no spatial autocorrelation between ΔP50/ΔHSM and CWD at the 1.0° scale using Moran's I. All traits and predictors were z-score standardized based on the ΔP50 or ΔHSM mean and SD for each data subset and climate variable mean and SD for each grid subset, making effect sizes comparable across traits and predictors. We looked at the sensitivity of response coefficient magnitude and significance to plots with a minimum of 80% trait coverage by basal area (61, 62) in the first inventory for our base-version trait dataset, the phylogenetically imputed version, and the strict quality control version (for P50 only).

To analyze the demographic drivers and quantify trait velocities of ΔP50 and ΔHSM, we used all plots with trait coverage by basal area fraction of >80% in the first inventory and linear models with ΔP50 or ΔHSM (in MPa y^{-1}) as the dependent variable and cumulative basal area mortality and date of the last census (39, 40) measurement as the independent variables. Finally, we quantified coordination between ΔP50 and ΔHSM using Spearman's ρ. Correlation coefficients and significance levels are presented in *SI Appendix*, Table S4.

Q-Q plots indicated overdispersion in both our trait-climate and trait-mortality models that could not be accounted for using transformations. Given the large sample size of FIA plots and the consensus that symmetric overdispersion does not tend to bias parameter estimates, only significance tests, we provide two estimates of response coefficient magnitude and significance for each dataset version, one estimate including the entire dataset, and one where we excluded outliers (identified as points with residuals >2σ from the mean). This methodology resulted in six estimates for response coefficients for P50 and four estimates for HSM. Coefficient estimates from each technique are grouped in Fig. 3 and recorded in *SI Appendix*, Tables S2 and S3 in the following order: 1) base-version trait dataset, 2) base-version trait dataset with outliers removed, 3) phylogenetically imputed version, 4) phylogenetically imputed version with outliers removed, 5) strict quality control version (for P50 only), and 6) strict quality control version (for P50 only) with outliers removed. We performed model selection using Akaike information criterion including all possible variable combinations, and model selection was performed using the MuMIn package (63). Statistical analyses were performed in the R statistical environment (64).

Data and Code Availability. All forest inventory plot data are publicly available at the US Forest Service's FIA program website <https://www.fia.fs.fed.us/>. Gridded trait maps are publically available at Figshare (DOI: 10.6084/m9. figshare.11962710).

1. P. B. Reich, The world-wide "fast-slow" plant economics spectrum: A traits manifesto. *J. Ecol.* **102**, 275–301 (2014).
2. W. R. Anderegg et al., Meta-analysis reveals that hydraulic traits explain cross-species patterns of drought-induced tree mortality across the globe. *Proc. Natl. Acad. Sci. U.S.A.* **113**, 5024–5029 (2016).
3. W. R. L. Anderegg et al., Hydraulic diversity of forests regulates ecosystem resilience during drought. *Nature* **561**, 538–541 (2018).
4. J. C. Domec et al., Conversion of natural forests to managed forest plantations decreases tree resistance to prolonged droughts. *For. Ecol. Manage.* **355**, 58–71 (2015).

5. W. R. L. Anderegg, A. T. Trugman, D. R. Bowling, G. Salvucci, S. E. Tuttle, Plant functional traits and climate influence drought intensification and land-atmosphere feedbacks. *Proc. Natl. Acad. Sci. U.S.A.* **116**, 14071–14076 (2019).

6. G. Bonan, Forests and climate change: Forcings, feedbacks, and the climate benefits of forests. *Science* **320**, 1444–1449 (2008).

7. A. Berg *et al.*, Land–atmosphere feedbacks amplify aridity increase over land under global warming. *Nat. Clim. Chang.* **6**, 869–874 (2016).

8. S. I. Seneviratne *et al.*, Investigating soil moisture-climate interactions in a changing climate: A review. *Earth Sci. Rev.* **99**, 125–161 (2010).

9. L. D. L. Anderegg, J. HilleRisLambers, Local range boundaries vs. large-scale trade-offs: Climatic and competitive constraints on tree growth. *Ecol. Lett.* **22**, 787–796 (2019).

10. P. B. Adler, J. HilleRisLambers, The influence of climate and species composition on the population dynamics of ten prairie forbs. *Ecology* **89**, 3049–3060 (2008).

11. C. D. Allen, D. D. Breshears, Drought-induced shift of a forest-woodland ecotone: Rapid landscape response to climate variation. *Proc. Natl. Acad. Sci. U.S.A.* **95**, 14839–14842 (1998).

12. J. Lenoir, J. C. Gégout, P. A. Marquet, P. De Ruffray, H. Brisse, A significant upward shift in plant species optimum elevation during the 20th century. *Science* **320**, 1768–1771 (2008).

13. A. Esquivel-Muelbert *et al.*, Compositional response of Amazon forests to climate change. *Glob. Change Biol.* **25**, 39–56 (2019).

14. A. E. Kelly, M. L. Goulden, Rapid shifts in plant distribution with recent climate change. *Proc. Natl. Acad. Sci. U.S.A.* **105**, 11823–11826 (2008).

15. S. Fauset *et al.*, Drought-induced shifts in the floristic and functional composition of tropical forests in Ghana. *Ecol. Lett.* **15**, 1120–1129 (2012).

16. F. M. Hoffman *et al.*, Causes and implications of persistent atmospheric carbon dioxide biases in Earth System Models. *J. Geophys. Res. Biogeosci.* **119**, 141–162 (2014).

17. A. Dai, Increasing drought under global warming in observations and models. *Nat. Clim. Chang.* **3**, 52–58 (2012).

18. A. P. Williams *et al.*, Temperature as a potent driver of regional forest drought stress and tree mortality. *Nat. Clim. Chang.* **3**, 292–297 (2012).

19. M. Reichstein *et al.*, Climate extremes and the carbon cycle. *Nature* **500**, 287–295 (2013).

20. P. Ciais *et al.*, "Carbon and other biogeochemical cycles" in *Climate Change 2013: The Physical Science Basis. Contribution of the Working Group I to the Fifth Assessment Report of the Intergovernmental Panel on Climate Change*, T. F. Stocker *et al.*, Eds. (Cambridge Univ Press Cambridge, New York, 2013), pp. 465–570.

21. N. E. Zimmermann *et al.*, Climatic extremes improve predictions of spatial patterns of tree species. *Proc. Natl. Acad. Sci. U.S.A.* **106** (suppl. 2), 19723–19728 (2009).

22. T. L. Root *et al.*, Fingerprints of global warming on wild animals and plants. *Nature* **421**, 57–60 (2003).

23. M. W. Tingley, M. S. Koo, C. Moritz, A. C. Rush, S. R. Beissinger, The push and pull of climate change causes heterogeneous shifts in avian elevational ranges. *Glob. Change Biol.* **18**, 3279–3290 (2012).

24. R. J. Wilson, D. Gutiérrez, J. Gutiérrez, V. J. Monserrat, An elevational shift in butterfly species richness and composition accompanying recent climate change. *Glob. Change Biol.* **13**, 1873–1887 (2007).

25. P. G. Jarvis, The interpretation of the variations in leaf water potential and stomatal conductance found in canopies in the field. *Philos Trans R Soc B Biol Sci* **273**, 593–610 (1976).

26. D. Kennedy *et al.*, Implementing plant hydraulics in the community land model, version 5. *J. Adv. Model. Earth Syst.* **11**, 485–513 (2019).

27. X. Xu, D. Medvigy, J. S. Powers, J. M. Becknell, K. Guan, Diversity in plant hydraulic traits explains seasonal and inter-annual variations of vegetation dynamics in seasonally dry tropical forests. *New Phytol.* **212**, 80–95 (2016).

28. C. Henry *et al.*, A stomatal safety-efficiency trade-off constrains responses to leaf dehydration. *Nat. Commun.* **10**, 3398 (2019).

29. D. M. Johnson *et al.*, Co-occurring woody species have diverse hydraulic strategies and mortality rates during an extreme drought. *Plant Cell Environ.* **41**, 576–588 (2018).

30. S. M. Gleason *et al.*, Weak tradeoff between xylem safety and xylem-specific hydraulic efficiency across the world's woody plant species. *New Phytol.* **209**, 123–136 (2016).

31. A. J. R. Gillespie, Rationale for a national annual forest inventory program. *J. For.* **97**, 16–20 (1999).

32. J. T. Abatzoglou, S. Z. Dobrowski, S. A. Parks, K. C. Hegewisch, TerraClimate, a high-resolution global dataset of monthly climate and climatic water balance from 1958-2015. *Sci. Data* **5**, 170191 (2018).

33. H. Maherali, C. E. Moura, M. C. Caldeira, C. J. Willson, R. B. Jackson, Functional coordination between leaf gas exchange and vulnerability to xylem cavitation in temperate forest trees. *Plant Cell Environ.* **29**, 571–583 (2006).

34. K. R. Hultine *et al.*, Influence of soil texture on hydraulic properties and water relations of a dominant warm-desert phreatophyte. *Tree Physiol.* **26**, 313–323 (2006).

35. W. T. Pockman, J. S. Sperry, Vulnerability to xylem cavitation and the distribution of Sonoran Desert vegetation. *Am. J. Bot.* **87**, 1287–1299 (2000).

36. W. S. Phillips, Depth of roots in soil. *Ecology* **44**, (1963).

37. V. Devictor *et al.*, Spatial mismatch and congruence between taxonomic, phylogenetic and functional diversity: The need for integrative conservation strategies in a changing world. *Ecol. Lett.* **13**, 1030–1040 (2010).

38. Z. Yang *et al.*, The effect of environmental heterogeneity on species richness depends on community position along the environmental gradient. *Sci. Rep.* **5**, 15723 (2015).

39. A. T. Trugman, D. Medvigy, W. R. L. Anderegg, S. W. Pacala, Differential declines in Alaskan boreal forest vitality related to climate and competition. *Glob. Chang. Biol.* **24**, 1097–1107 (2018).

40. J. P. van Mantgem *et al.*, Widespread increase of tree mortality rates in the Western United States. *Science* **323**, 521–524 (2009).

41. A. D. Bjorkman *et al.*, Plant functional trait change across a warming tundra biome. *Nature* **562**, 57–62 (2018).

42. B. J. Enquist *et al.*, Assessing trait-based scaling theory in tropical forests spanning a broad temperature gradient. *Glob. Ecol. Biogeogr.* **26**, 1357–1373 (2017).

43. G. J. Nowacki, M. D. Abrams, The demise of fire and "Mesophication" of forests in the Eastern United States. *Bioscience* **58**, 123–138 (2008).

44. K. Raffa *et al.*, Cross-scale drivers of natural disturbances prone to anthropogenic amplification: The dynamics of bark beetle eruptions. *Bioscience* **58**, 501–517 (2008).

45. B. J. Bentz *et al.*, Climate change and bark beetles of the Western United States and Canada: Direct and indirect effects. *Bioscience* **60**, 602–613 (2010).

46. M. L. Gaylord *et al.*, Drought predisposes piñon-juniper woodlands to insect attacks and mortality. *New Phytol.* **198**, 567–578 (2013).

47. T. Zhang, Ü. Niinemets, J. Sheffield, J. W. Lichstein, Shifts in tree functional composition amplify the response of forest biomass to climate. *Nature* **556**, 99–102 (2018).

48. L. D. L. Anderegg *et al.*, Within-species patterns challenge our understanding of the leaf economics spectrum. *Ecol. Lett.* **21**, 734–744 (2018).

49. M. K. Bartlett *et al.*, Global analysis of plasticity in turgor loss point, a key drought tolerance trait. *Ecol. Lett.* **17**, 1580–1590 (2014).

50. A. Trugman *et al.*, *Climate and Plant Trait Strategies Determine Tree Carbon Allocation to Leaves and Mediate Future Forest Productivity* (Glob Chang Biol, 2019).

51. B. Choat *et al.*, Global convergence in the vulnerability of forests to drought. *Nature* **491**, 752–755 (2012).

52. M. P. Peters, L. R. Iverson, S. N. Matthews, Long-term droughtiness and drought tolerance of eastern US forests over five decades. *For. Ecol. Manage.* **345**, 56–64 (2015).

53. A. T. Trugman, L. D. L. Anderegg, J. S. Shaw, W. R. L. Anderegg, Dataset: Trait velocities reveal that mortality has driven widespread coordinated shifts in forest hydraulic trait composition. Figshare. https://doi.org/10.6084/m9.figshare.11962710. Deposited 10 March 2020.

54. S. R. Loarie *et al.*, The velocity of climate change. *Nature* **462**, 1052–1055 (2009).

55. W. A. Bechold, P. L. Patterson, "The enhanced forest inventory and analysis program - national sampling design and estimation procedures" (Gen Tech. Rep. SRS-80, NC US Department Agriculture Forest Service Southern Research Station, Asheville, 2005), p. 85.

56. M. D. Venturas *et al.*, Direct comparison of four methods to construct xylem vulnerability curves: Differences among techniques are linked to vessel network characteristics. *Plant Cell Environ.* **42**, 2422–2436 (2019).

57. R. P. Skelton *et al.*, Low vulnerability to xylem embolism in leaves and stems of north american oaks. *Plant Physiol.* **177**, 1066–1077 (2018).

58. N. G. Swenson, Phylogenetic imputation of plant functional trait databases. *Ecography* **37**, 105–110 (2014).

59. J. J. Wiens *et al.*, Niche conservatism as an emerging principle in ecology and conservation biology. *Ecol. Lett.* **13**, 1310–1324 (2010).

60. S. Chamberlain, Brranching: Fetch "Phylogenies" from Many Sources. R Package Version 040. https://CRANR-project.org/package=brranching. Accessed 4 August 2019.

61. E. Garnier *et al.*, Plant functional markers capture ecosystem properties during secondary succession. *Ecology* **85**, 2630–2637 (2004).

62. S. Taugourdeau, J. Villerd, S. Plantureux, O. Huguenin-Elie, B. Amiaud, Filling the gap in functional trait databases: Use of ecological hypotheses to replace missing data. *Ecol. Evol.* **4**, 944–958 (2014).

63. B. Kamil, MuMIn: Multi-Model Inference. R Package Version 1.15.6. https://CRAN.R-project.org/package=MuMIn. Accessed 17 March 2020.

64. R CT, R: A Language and Environment for Statistical Computing (Version 3.2.4, R Foundation for Statistical Computing, Vienna, Austria, 2016).